

Innovative dielectric elastomer actuator driver based on salamander muscle structures

Chenghong Zhang(张成红)

Citation: Chin. Phys. B, 2025, 34 (**10**): 104503. DOI: 10.1088/1674-1056/ae030a
http://cpb.iphy.ac.cn; http://iopscience.iop.org/cpb

What follows is a list of articles you may be interested in

Performance of tubular actuators constructed with dielectric elastomer materials

Chengguang Zhang(张成光)
Chin. Phys. B, 2025, 34 (**7**): 074501. DOI: 10.1088/1674-1056/add007

Nonlinear control of spacecraft formation flying with disturbance rejection and collision avoidance

Qing Ni(倪庆), Yi-Yong Huang(黄奕勇), Xiao-Qian Chen(陈小前)
Chin. Phys. B, 2017, 26 (**1**): 014502. DOI: 10.1088/1674-1056/26/1/014502

Reactionless robust finite-time control for manipulation of passive objects by free-floating space robots

Guo Sheng-Peng (郭胜鹏), Li Dong-Xu (李东旭), Meng Yun-He (孟云鹤), Fan Cai-Zhi (范才智)
Chin. Phys. B, 2014, 23 (**5**): 054502. DOI: 10.1088/1674-1056/23/5/054502

Innovative dielectric elastomer actuator driver based on salamander muscle structures

Chenghong Zhang(张成红)[1,2,†]

[1] *Key Laboratory of Advanced Manufacturing Technology, Ministry of Education, Guizhou University, Guiyang* 550025, *China*
[2] *School of Electronics & Information Engineering, Guiyang University, Guiyang* 550005, *China*

(Received 24 May 2025; revised manuscript received 9 August 2025; accepted manuscript online 4 September 2025)

Salamander robots represent an innovative class of crawling robots that combine flexible limbs and spines to achieve exceptional motion stability and adaptability in unstructured environments. These biomimetic systems employ soft actuators that replicate the smooth, organic movements of living organisms, significantly enhancing fluid interaction efficiency and propulsion performance. This research specifically focuses on improving dielectric elastomer actuator (DEA)-based fish-like underwater robots by developing a novel drive mechanism inspired by the salamander musculature. While aquatic organisms such as fish possess complex muscle structures that challenge direct imitation, salamanders offer a more tractable model due to their simpler anatomical organization. Notably, the lateral inferior axonal muscles in salamanders exhibit a nearly flat configuration, with myomangial membranes arranged in a linear distribution from the lateral midline to the abdominal midline — a structural feature that is particularly amenable to DEA replication. Through systematic analysis of salamander morphology, this study develops a DEA driver model that investigates two critical performance parameters: (i) the impact of electrode geometry on the bending angle; and (ii) the relationship between driver quantity and angular displacement. The experimental results confirm that DEAs mimicking salamander muscle architecture can achieve substantially increased bending angles under optimized conditions, thereby demonstrating measurable improvements in robotic propulsion capabilities.

Keywords: biomimetics, elastomer actuators (DEAs), robotics, muscle structure imitation

PACS: 45.40.Ln, 47.54.Jk, 61.41.+e, 77.84.–s

DOI: 10.1088/1674-1056/ae030a **CSTR:** 32038.14.CPB.ae030a

1. Introduction

As technological advancements continue, robotic tasks have grown increasingly sophisticated. To execute these complex operations in real-world environments, researchers have developed bionic robots that mimic living organisms. These biologically inspired robots have diverse applications across multiple fields. Humanoid bipedal robots and single-legged jumping robots have demonstrated remarkable mobility in obstacle-rich and uneven terrains.[1] Aquatic exploration has been enhanced by fish-inspired swimming robots capable of navigating oceans, rivers, and reservoirs.[2] Similarly, snake-like robots and other crawling designs exhibit exceptional versatility, moving through confined spaces on land while maintaining aquatic mobility.[3,4] In vertebrate locomotion studies, salamander robots have emerged as particularly significant in recent years.[6] Given the status of salamanders as among the earliest terrestrial vertebrates,[8] these robotic models serve as valuable tools for testing biological hypotheses about the evolution of animal movement.[6,7]

Salamanders possess distinctive morphological characteristics that contribute to their remarkable locomotion capabilities. Their slender bodies and flexible limbs enable a unique movement pattern in which limb–ground interactions coordinate with spinal undulations. This biomechanical design results in several advantageous features: (i) the body maintains continuous ground contact, creating a low center of gravity; (ii) the relatively large support surface enhances stability during crawling; and (iii) these combined attributes allow effective navigation through complex terrains, including swamps and hilly environments. These biological advantages have inspired the development of salamander robots, which replicate the flexibility of animal movement for operation in unstructured environments. Modern salamander robots incorporate two key design elements: (i) a flexible spinal structure that mimics biological undulation; and (ii) specialized limb configurations that assist in locomotion. Typical implementations feature short limbs with specific orientations — upper limbs parallel to the ground, and lower limbs perpendicularly — which maintain the robot's low center of gravity and ensure movement stability comparable to that of its biological counterparts.[8–10]

The evolutionary development of salamander robots at École Polytechnique Fédérale de Lausanne (EPFL) has led to significant technological progress across multiple generations. Figure 1 depicts the pioneering model, which adapted its body structure from the snake-inspired AmphiBot I,[11] featuring limbs with single degrees of freedom.[12,13] Subsequent iterations resulted in marked improvements. Figure 2 illus-

†Corresponding author. E-mail: zhangchenghongcn@aliyun.com

© 2025 Chinese Physical Society and IOP Publishing Ltd. All rights, including for text and data mining, AI training, and similar technologies, are reserved.

trates the first-generation salamander robot with enhanced installation methods, circuit reliability, and water resistance,[14] whereas figure 3 presents the second-generation model specifically designed to investigate the relationship between limb dimensions/swing amplitude and locomotion efficiency.[15] The current pinnacle of this developmental lineage is Pleurobot,[16] representing the most biologically accurate replication of salamander skeletal structures to date.



Fig. 1. Salamandra robotica.

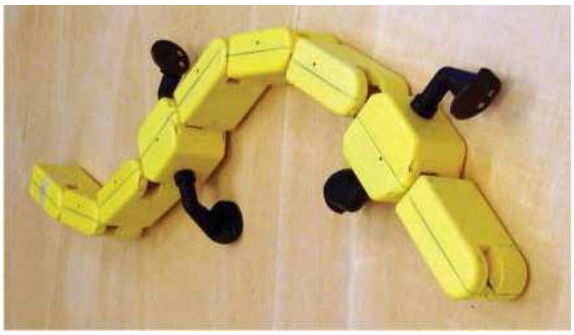


Fig. 2. Salamandra robotica I.



Fig. 3. Salamandra robotica II.

This research focuses on optimizing the propulsion system of salamandra robotic robots through innovative dielectric elastomer (DE)-based drive mechanisms. By conducting a thorough biomechanical analysis of salamander musculature, we engineered a DEA that precisely replicates the creatures' distinctive movement patterns. The developed DEA demonstrates two key advancements: (i) significantly improved propulsion efficiency in robotic applications; and (ii) novel capabilities for investigating fundamental principles of vertebrate locomotion. This dual-focused approach not only pushes the boundaries of bionic robotics, but also establishes a groundbreaking platform for studying evolutionary biomechanics.

2. Dielectric elastomer drive principle

Among various electronic electroactive polymers, DEs stand out as exceptional driving materials for soft actuators. These DE-based systems offer three key advantages: (i) high power density, (ii) rapid response speed, and (iii) excellent driving stability. Their mechanical properties closely resemble those of human tissues, particularly in demonstrating stress-strain relationships analogous to those of natural muscles. This biomimetic characteristic makes DEs particularly suitable for artificial muscle applications and soft robotics. DEAs achieve an energy efficiency of 26%, which is comparable to the 20% efficiency of human muscle.[17]

The electrode formation mechanism of DEs operates through two primary effects: electropolarization and electroelastic effects (Fig. 2(a)). While DEs are inherently nonconductive, their functional capability emerges when electrode materials coat both surfaces, creating a parallel plate capacitor with a characteristic "sandwich" structure. Under applied electric fields, this configuration results in the following: (i) polarization: DE molecules align, causing volumetric and shape changes; (ii) interactions: like-surface charges repel, whereas opposite-surface charges attract, generating Maxwell stress; (iii) changes: Macroscopic compression along the thickness (z-axis) with simultaneous expansion in the planar (xy) directions. The deformation magnitude and orientation can be precisely controlled through electric-field parameters. Notably, this process is fully reversible: removing the electric field returns the dielectric material to its initial state, enabling cyclic actuation. The resulting Maxwell stress (p) and thickness-direction strain (s) is quantitatively described in Ref. [18], with the complete driving principle illustrated in Fig. 4.

$$p = \varepsilon_0 \varepsilon_r E^2, \tag{1}$$

$$s = \frac{\varepsilon_0 \varepsilon_r E^2}{Y}, \tag{2}$$

where ε and ε_r are the vacuum dielectric constant and the relative dielectric constant, respectively, and E and Y are the electric field strength and the elastic modulus, respectively. The dielectric constant, elastic modulus and breakdown strength are the main factors affecting DE performance and the key factors determining DEA-driven deformation.

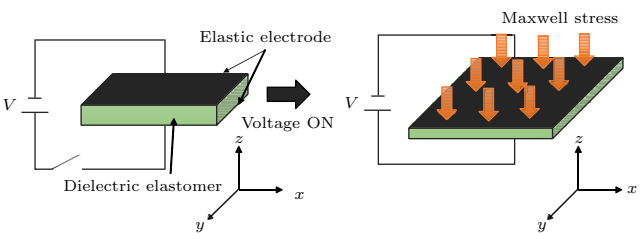


Fig. 4. The DE driving principle.

3. Muscle structure of salamanders

Salamanders, as aquatic creatures, have a unique muscle structure that provides a solid foundation for their flexible ability to swim in water. The muscle structure of salamanders can be divided into the following characteristics.

(i) Distribution of muscle mass The salamander muscles extend from the head all the way to the tail, and these muscle masses are separated by myosepta, forming a distinct segmented structure. The muscle structure is shown in Fig. 5.

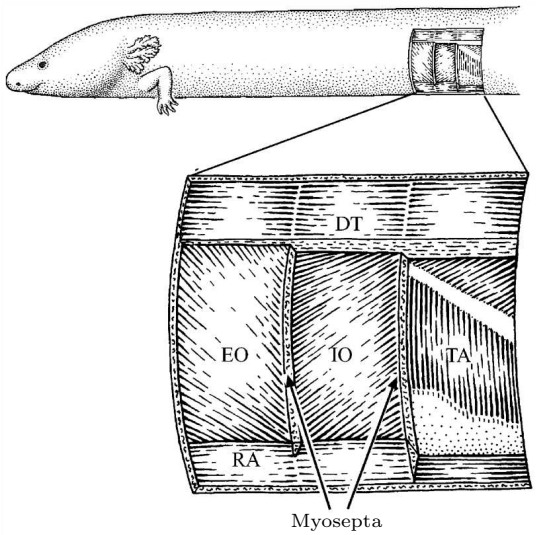


Fig. 5. A lateral view of the axial musculature of Siren lacertina. Abbreviations: DT, dorsalis trunci; EO, external oblique; IO, internal oblique; RA, rectus abdominis; TA, transverse abdominis.

(ii) Muscle fiber angles When there is no movement, the muscle fibers within the block are roughly arranged at a 45° angle in the direction of length, which helps to produce efficient muscle contraction and extension during movement.

(iii) Symmetry When the salamander is placed on a plane perpendicular to the spine, the muscle structure clearly extends symmetrically from the spine to the skin, and this symmetry ensures that the salamander can maintain balance and stability while swimming.

(iv) Cross-sectional structure When viewed from a cross-section, the salamander's muscle structure is more complex and orderly, with different muscle blocks and muscle fibers that are interwoven to form its powerful motor system. The cross-section of the salamander is shown in Fig. 6.

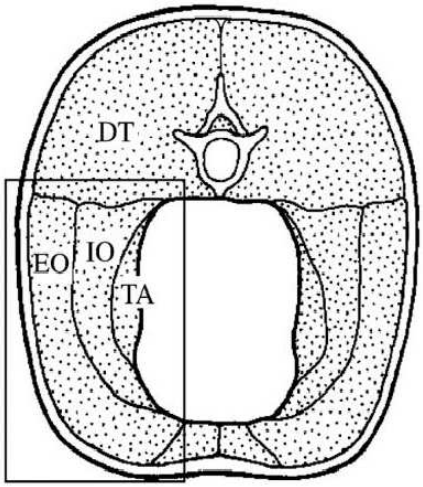


Fig. 6. A cross-sectional view of the salamander.

In summary, the muscle structure of salamanders is characterized by segmentation, angular arrangement, symmetry and a complex cross-sectional structure, which together provide them with the ability to swim efficiently in water.

4. Drive unit

4.1. Design of the driver unit

The design uses 3D-printed pillars to replicate the function of collagen-like membranes that separate muscle segments in salamanders. These precisely fabricated pillars are integrated with a carbon-fiber–reinforced plastic (CFRP) spinal simulation structure, effectively mimicking both the structural separation and mechanical support between adjacent muscle blocks observed in biological systems.

The prestretched dielectric elastomers (DEs) are aligned parallel to the spinal simulation structure, effectively mimicking the continuous muscle fiber arrangement observed in salamanders from the spine to the skin. This prestretching process serves two key functions: (i) it reduces the DEA thickness, allowing greater Maxwell stress generation upon voltage application, thereby enhancing drive performance; and (ii) it creates a built-in antagonistic mechanism where the prestretched DEA maintains contraction through restoring forces prior to activation, while the applied voltage induces stretching via Maxwell stress. This dual-state design precisely replicates the antagonistic muscle behavior that is fundamental to salamander locomotion.

4.2. Physical drive unit

The physical driver is shown in Fig. 7.

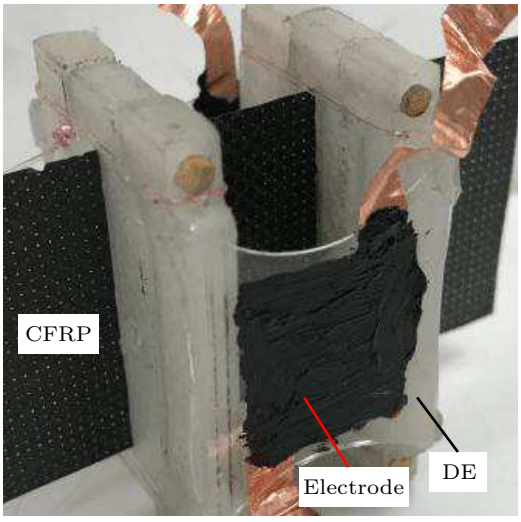


Fig. 7. The physical view of the driver unit.

Figure 7 presents the physical implementation of the driver unit, featuring a dielectric elastomer actuator (DEA) constructed with 3 M VHB acrylic foam adhesive tape. The DEA undergoes optimized biaxial prestretching — 400% in

the vertical (body height) direction and 300% in the longitudinal (body length) direction — to enhance its electromechanical performance. The system employs carbon grease as a flexible electrode material, complemented by copper tape terminals to ensure robust electrical connectivity. This configuration achieves two key functional outcomes: (i) precise simulation of salamander muscle antagonism through voltage-controlled deformation; and (ii) programmable bending kinematics, where both the magnitude and direction of movement can be dynamically adjusted via applied voltage parameters.

5. Changes in the shape of the DEA electrode to the bending angle

To investigate how electrode geometry affects actuator performance, this study experimentally evaluated whether mimicking salamander muscle fiber angles in DEA electrode shapes could enhance the bending angle of the driver unit. This research specifically examined the relationship between flexible electrode configurations and their resulting bending angles.

5.1. Flexible electrode shape

To systematically evaluate the impact of flexible electrode geometry on driver unit performance, we developed three distinct electrode configurations for experimental testing. These specially designed electrode patterns, illustrated in Fig. 8, were implemented on the DEAs to quantify their influence on the bending-angle characteristics.

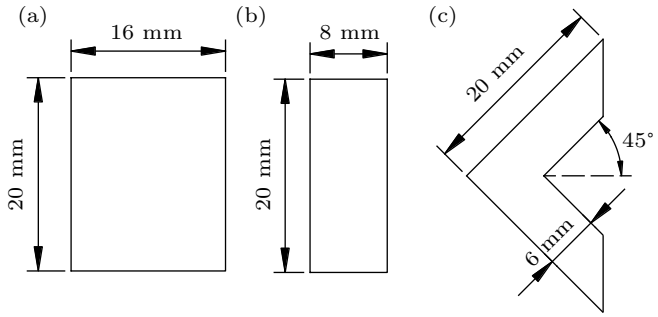


Fig. 8. The shape of the flexible electrode used in the experiment.

Electrode shape A is the maximum rectangular area that can be coated on the dielectric elastomer at the driver-unit size set in this experiment. Electrode shape B is "L" shaped, inspired by the orientation of salamander muscle fibers. The central narrow part is symmetrical from top to bottom, and the symmetry line is parallel to the long-axis direction of the unit. The opening angle of the electrodes mimics the initial angle of the salamander muscle fibers, with a 45° tilt in the long-axis direction. Electrode shape C is a rectangular electrode with the same area as shape B. The main purpose of the design is to evaluate the effect of the electrode shape on the bending angle individually, excluding the area factor. The effect of the shape of the flexible electrode on the bending angle of the driver unit was analyzed by comparing the bending angle performance of three different shapes of flexible electrodes under the same experimental conditions.

5.2. Measurement results of bending angles

A sinusoidal wave with a frequency of 0.1 Hz is applied to the driver unit of the flexible electrode shape shown in Fig. 9, varying from 0 to 4 kV, to the DEA on both sides of the driver unit. The phase difference between the two DEAs is 180° to ensure that when the maximum voltage is applied to one DEA, the voltage is not applied to the other. This alternating activation creates a left-right bending motion in the drive unit.

The bending motion is captured from a top-view perspective, enabling precise measurement of the reference plane's bending angle (θ). To account for the DE's viscoelastic properties, coordinate measurements are taken after a 60 second stabilization period following voltage application. For statistical reliability, three measurements are conducted per flexible electrode, with all video-recorded data subsequently averaged to determine the mean bending angle of each unit.

Figure 9 shows the time-dependent bending angles produced by drive units with three different electrode configurations. The initial state of the driver unit slightly deviates from perfect alignment due to manufacturing tolerances, including variations in the restoring force of prestretched dielectric elastomers on both sides and minor dimensional inaccuracies in the supporting pillars. Consequently, the baseline measurement (median waveform value) exhibits a nonzero offset.

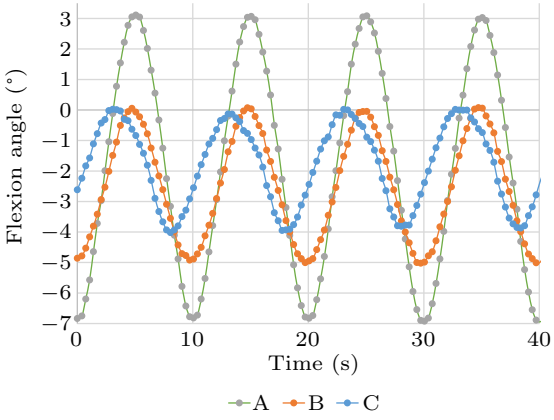


Fig. 9. Bending angle variation over time for different flexible electrode shapes.

The experimental results demonstrate significant variations in bending performance among three electrode configurations (A, B, C) in dielectric elastomer actuators (DEAs) mimicking salamander muscle structures. Electrode A, with the largest rectangular area achievable for the drive unit, achieved the highest bending angle of 4.87°, surpassing that of the natural salamander swimming bend ($\sim$4.0°). This highlights its superior practical applicability, as larger electrode areas maximize deformation under electric fields. In contrast, electrodes B (2.51°) and C (1.97°), despite having identical

areas, exhibited divergent performances due to shape differences. Electrode C's "L"-shaped design, inspired by the 45° tilt of salamander muscle fibers, underperformed because its uniform expansion failed to replicate the dynamic strain amplification of biological muscle contraction. Moreover, electrode B's rectangular shape outperformed C, confirming that the electrode geometry — independent of area — critically influences the bending efficiency.

These findings challenge initial assumptions: while biomimicry of muscle fiber angles (electrode C) seems theoretically advantageous, practical performance favors simpler larger-area designs (electrode A). This suggests that for DEA-driven robotics, electrode area optimization outweighs strict anatomical mimicry. Furthermore, electrode A's ability to exceed biological benchmarks (4.87° vs. 4.0°) underscores its potential for high-performance soft robotics in unstructured environments. Future work could explore hybrid designs that combine large-area electrodes with localized angle variations to bridge the gap between biomimicry and electromechanical efficiency.

6. Bending angles based on quantity variations of DEA

To imitate the parallel and continuous arrangement of muscle fibers from the spine to the skin, the salamander muscle structure is achieved by increasing the number of DEAs used by the driving unit from the coronal plane of the salamander's back and abdomen.

6.1. Increasing the number of DEAs used in the drive unit

To imitate the salamander muscle fiber structure arranged parallel from the spine to the skin more precisely, two drive unit configurations for increasing the amount of dielectric elastomer (DE) used were designed: parallel arrangement and stacked arrangement.

(i) Parallel arrangement of the DEA drive units A parallel arrangement means arranging the DEAs in a spaced manner within the drive unit. We made two parallel arrangements of drive units, with 2 and 3 DEAs on one side. This arrangement ensures that there is a certain interval between the DEAs, avoiding the degradation of drive performance due to excessive density. The parallel arrangement is shown in Fig. 10.

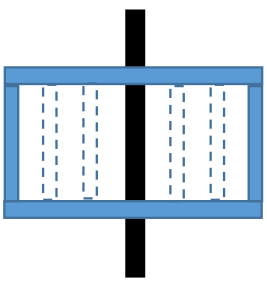


Fig. 10. The parallel arrangement of the DEA drive units.

(ii) Stacked DEA driver units. The stacked arrangement alternately overlaps and closely attaches the DEAs used for the drive unit with the elastomer and the flexible electrode. This arrangement enhances drive performance by increasing the number of DEA layers, but it may also generate additional resistance due to interlayer adhesive forces, affecting the flexibility of movement.

6.2. Driver unit test results

Experiments were conducted on the variation in the buckling angle with the voltage frequency when the number and configuration of DEAs in the driver unit were changed. In the experiment, the buckling angles of five different driver configurations were measured: a driver configured with one DEA, a driver configured with two or three DEAs in parallel, and a driver configured with two or three DEAs in layers. The conditions of the experiment were as follows: a maximum voltage of 4.0 kV was applied in the form of a sine wave; the frequencies were 0.1 Hz, 0.5 Hz, 1.0 Hz, 2.0 Hz, 3.0 Hz, 4.0 Hz, and 5.0 Hz. The phase difference between the left and right DEAs of the drive unit was set at 180°.

The maximum frequency buckling angles of each driver are shown in Fig. 11. The comparison gain of the bending angles of the drivers at each frequency with the measured bending angle at 0.1 Hz as the reference is shown in Fig. 12.

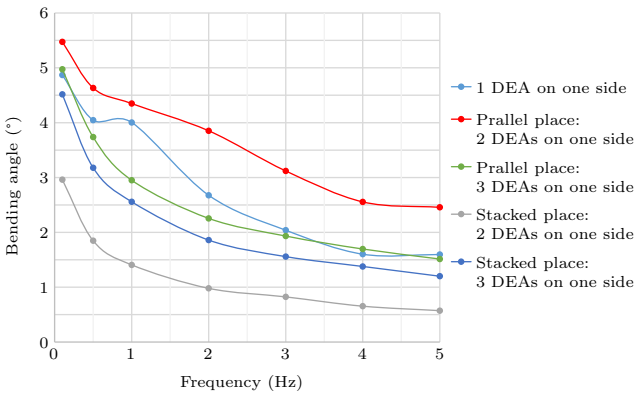


Fig. 11. The maximum bending angles corresponding to the frequencies of each driver unit.

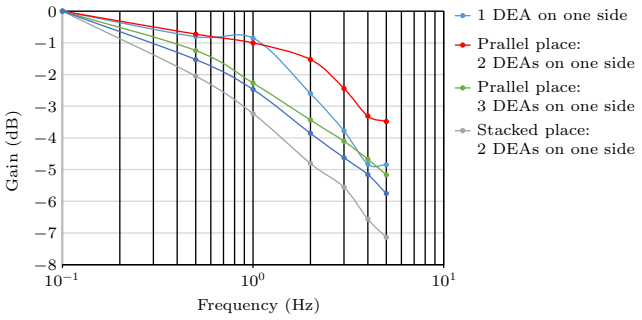


Fig. 12. The gains corresponding to the frequencies of each drive unit.

The cutoff frequencies corresponding to half of the bending angle at a drive frequency of 0.1 Hz are shown in Table 1. Notably, the gain of the cutoff frequency at this time is −3 dB.

Table 1. The cutoff frequencies for each driver unit.

DEA configuration types	–	Parallel configuration	Parallel configuration	Stacked configuration	Stacked configuration
Number of DEA on one side	1	2	3	2	3
Cutoff frequency (Hz)	2.68	3.95	1.29	0.71	1.02

The experimental results demonstrate a clear performance advantage of configurations over configurations in dielectric elastomer actuator (DEA) drive units. Across all the tested frequencies, parallel arrangements consistently achieve larger bending angles. This superiority stems from the inherent limitations of stacked designs: the bonding between elastomer layers introduces additional drag during deformation, which impedes movement and reduces bending efficiency. In contrast, parallel configurations maintain optimal spacing between DEAs, minimizing interference and maximizing the actuation potential.

When comparing parallel configurations with versus three DEAs, the data reveal nuanced trade-offs.

Bending angle At 0.1 Hz, the two-DEA unit achieves a bending angle of 5.47°, outperforming the three-DEA unit (4.97°). This 1.10× advantage persists across other frequencies, with the two-DEA configuration bending 2.98× moreat cutoff frequencies. The reduced bending in the three DEA units likely results from increased rigidity, which alters the force balance under voltage application.

Force generation vs. flexibility While adding DEAs enhances the force output, it also stiffens the unit, compromising the bending performance. This suggests a design trade-off between power and flexibility.

The study highlights a critical relationship between DEA quantity and responsiveness. Increasing the number of DEAs from two to three in parallel configurations reduces the cutoff frequency, which is attributed to the longer lever arm position of additional DEAs. This diminishes the force generation efficiency and amplifies viscous effects. However, the two-DEA unit maintains a 1.47× higher cutoff frequency than single-DEA designs do, indicating improved responsiveness despite increased viscoelasticity.

The results underscore the importance of configuration and quantity optimization in DEA-based actuator design, particularly for applications requiring precise bending control and dynamic response. The two-DEA parallel configuration emerges as the most effective design choice, balancing bending performance with mechanical responsiveness.

7. DEA configuration for variations in the bending angle and force

Placing a DEA within the drive unit closer to the CFRP of the spine results in a greater bending angle. The effects of the configuration position of the DEA on the bending angle and force generation of the drive unit are studied to create a drive unit that can achieve a greater bending angle.

7.1. Manufacturing the drive unit

To enhance the drive unit's bending performance, we strategically repositioned the DEA closer to the central axis of the drive unit, aligning it with the spinal simulation structure. Recognizing that this positional adjustment might reduce force output, we implemented a parallel arrangement of multiple DEAs as a compensatory measure. Three distinct drive-unit configurations were developed, incorporating 1, 2, and 3 parallel DEAs.

As detailed in Table 2, the force generation exhibited a nonlinear relationship with the number of DEAs. The 2-DEA configuration demonstrated superior performance, producing a 1.19 times greater force than the 3-DEA arrangement and a 2.43 times greater force than the single DEA configuration.

Table 2. The force of each drive unit.

DEA configuration type	–	Parallel arrangement	Parallel arrangement
Number of DEAs on one side of the unit	1	2	3
Force (mN)	33.5	40.6	82.1

The final drive unit prototype (shown in Fig. 13) was fabricated via three DEA sheets positioned along the side of the structure, with their configuration moving closer to the spinal component. This modified design features two key improvements over the traditional parallel configuration with three side-mounted DEAs: (i) the inter-DEA spacing was reduced by 50%, while (ii) the original distance from the spine was maintained. This optimized arrangement enhances the unit's performance while preserving structural integrity.

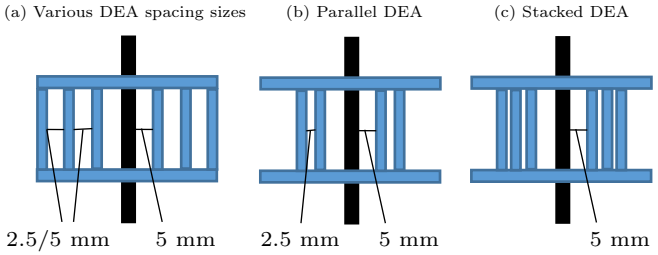


Fig. 13. The DEA configurations.

For comparative analysis, the study examines drive units with two configurations: (i) a parallel arrangement using two DEAs at the maximum bending angle to investigate DEA quantity effects; and (ii) a stacked three-DEA configuration that eliminates inter-DEA spacing. This stacked design positions each DEA closer to the central spine while reducing the CFRP distance more effectively than traditional approaches.

7.2. Results of the drive experiment

To assess the bending performance across frequencies, each drive unit underwent testing under the following conditions: application of a 4 kV sinusoidal voltage at seven discrete frequencies (0.1 Hz, 0.5 Hz, 1.0 Hz, 2.0 Hz, 3.0 Hz, 4.0 Hz, and 5.0 Hz) with a 180° phase difference maintained between the left and right DEAs. Figure 14 shows the frequency-dependent maximum bending angles achieved by each driver configuration. For comparative analysis, figure 15 presents the normalized gain of each driver's bending angle relative to the 0.1 Hz reference conditions.

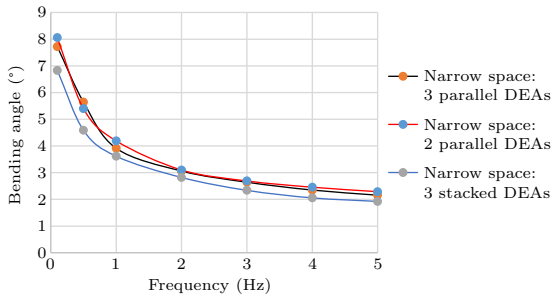


Fig. 14. The maximum buckling angles corresponding to the frequencies of each driver unit.

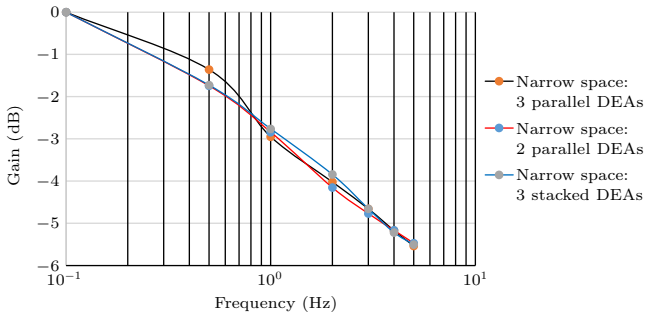


Fig. 15. Gain corresponding to the frequency of each driver unit.

Additionally, the cutoff frequencies associated with half the bending angle of each drive unit were measured at a driving frequency of 0.1 Hz, as presented in Table 3. The force generated by each driver unit is shown in Table 4.

Table 3. The cutoff frequency of each drive unit.

DEA configuration type	Parallel arrangement	Parallel arrangement	Stacked arrangement
Number of DEA on one side of the unit	3	2	3
Cutoff frequency (Hz)	0.94	1.00	0.97

Table 4. The force of each drive unit.

DEA configuration type	Parallel arrangement	Parallel arrangement	Stacked arrangement
Number of DEA on one side of the unit	3	2	3
Force (mN)	98.2	44.1	36.6

The experimental results demonstrate the critical role of the DEA configuration in determining both the angle and generation of the drive units. The force generated by each driver unit was measured at a drive frequency of 0.1 Hz when the bending angle reached its maximum. The most striking finding was that driving units with three DEAs arranged side by side and with reduced intervals produced the force of 97.9 mN. This force output was 2.26 times greater than that achieved by two DEAs arranged in parallel and 2.71 times greater than that of three DEAs arranged in a stacked configuration. These results underscore the importance of optimization of both the quantity and spatial arrangement of DEAs to enhance performance. By carefully adjusting these parameters, researchers can not only increase the bending angle of the drive unit but also boost its power generation capacity, leading to more efficient and effective robotic movement.

Further analysis revealed that a configuration — particularly when combined with to the spinal simulation structure — yields superior results. For example, a parallel arrangement with DEAs achieved a bending angle of 8.06° at 0.1 Hz, representing a 1.66-fold improvement over the initial prototype's value of 4.87°. This configuration strikes an optimal balance between and force generation, making it highly suitable for applications requiring precise and powerful actuation. The success of this design can be attributed to its ability to mimic the natural muscle structure of salamanders, where parallel muscle fibers work in harmony to produce coordinated movement.

However, the study also highlights the limitations of stacked configurations. While stacking DEAs could theoretically enhance performance by increasing the number of active layers, the experimental data revealed that adhesive forces introduce additional resistance, which negatively impacts both the bending angle and force output. This finding suggests that designs may not be ideal for applications where maximization of deformation and efficiency are priorities. Instead, future research should focus on refining configurations and exploring variables, such as spacing, prestretch ratios, and electrode shapes, to further optimize performance.

8. Conclusion

This study presents the development of an innovative dielectric elastomer actuator (DEA) driver designed to mimic the muscle structure of salamanders, with the primary goal to enhance the propulsion performance of fish-like underwater robots. Through a comprehensive analysis of salamander muscle characteristics, the research team successfully designed and fabricated a DEA driver capable of replicating the unique movement patterns of salamanders. The performance of this driver was systematically validated through a series of experiments, demonstrating its potential for practical applications in bionic robotics.

Central to the design are 3D-printed pillars that simulate the separation and support functions of salamander muscle blocks. These pillars are integrated with a spinal simu-

lation structure, onto which prestretched DEAs are mounted in parallel. This configuration effectively emulates the continuous muscle fibers that extend from the salamander's spine to its skin, enabling the driver to replicate the natural bending and undulating motions observed in salamanders during swimming.

This study investigated the impact of the electrode shape and DEA configuration on the driver's bending angle, revealing several critical insights.

(i) Electrode shape: Three distinct electrode shapes were tested, with the largest area electrode (shape A) producing a maximum bending angle of 4.87°. This performance surpasses the natural bending angle of swimming salamanders (approximately 4.0°) by a factor of 1.21, highlighting the effectiveness of the design.

(ii) DEA configuration: The parallel arrangement of DEAs outperforms the stacked configuration in terms of both the bending angle and responsiveness. For example, a driver unit with two DEAs in parallel achieved a bending angle of 8.06° when the spacing between DEAs was reduced — a 1.66-fold improvement over the initial prototype.

(iii) Proximity to the spine: Placing DEAs closer to the spinal simulation structure further increased the bending angle. However, this adjustment came at the cost of reduced force generation. To mitigate this, the team explored increasing the number of DEAs and reported that a unit with three DEAs generated a maximum force of 97.9 mN.

The findings of this study have significant implications for the field of bionic robotics. By successfully mimicking the muscle structure of salamanders, the DEA driver offers a novel solution for improving the propulsion efficiency of underwater robots. This research also provides valuable insights into the relationships among electrode design, the DEA configuration, and mechanical performance, which can inform future developments in soft robotics and biomimetic systems.

Moreover, the study underscores the potential of dielectric elastomers as versatile actuators for applications requiring high flexibility and responsiveness. The ability to fine-tune the driver's performance through adjustments in electrode shape and DEA arrangement opens new avenues for the optimization of robotic locomotion in diverse environments.

Acknowledgments

Project supported by the Joint Open Fund of Guizhou Provincial Department of Education (Grant No. [2022] 439) and the Doctoral Research Foundation of Guiyang University, China (Grant No. GYUKY-2025).

References

[1] Zhou X and Bi S 2012 *Bioinspir. Biomim.* **7** 041001
[2] Raj A and Thakur A 2016 *Bioinspir. Biomim.* **11** 031001
[3] Hirose S and Yamada H 2009 *IEEE Robot. Autom. Mag.* **16** 88
[4] Koh J S and Cho K J 2013 *IEEEASME Trans. Mechatron.* **18** 419
[5] Ashley-Ross M A and Bechtel B F 2004 *J. Exp. Biol.* **207** 461
[6] Gao K Q and Shubin N 2001 *Nature* **410** 574
[7] Crespi A, Karakasiliotis K, Guignard A and Ijspeert A J 2013 *IEEE Trans. Robot.* **29** 308
[8] Yamada H and Hirose S 2006 *J. Robot. Mechatron.* **18** 305
[9] Katz B, Carlo J D and Kim S 2019 *Proc. IEEE Int. Conf. Robot. Autom.* 6295
[10] Fankhauser P, Bjelonic M, Dario Bellicoso C, Miki T and Hutter M 2018 *Proc. IEEE Int. Conf. Robot. Autom.* 5761–5768
[11] Crespi A, Badertscher A, Guignard A and Ijspeert A J 2005 *Robot. Auton. Syst.* **50** 163
[12] Ijspeert A J, Crespi A and Cabelguen J M 2005 *Neuroinformatics* **3** 171
[13] Crespi A and Ijspeert A J 2009 *Artif. Life Models Hardw.* 35–64
[14] Ijspeert A J, Crespi A, Ryczko D and Cabelguen J M 2007 *Science* **315** 1416
[15] Karakasiliotis K and Ijspeert A J 2009 *IEEE/RSJ Int. Conf. Intell. Robot. Syst.* 5015–5020
[16] Karakasiliotis K, Thandiackal R, Melo K, Horvat T, Mahabadi N K, Tsitkov S, Cabelguen J M and Ijspeert A J 2016 *J. R. Soc. Interface* **13** 20151089
[17] Yang L, Wang H, Zhang D S, Yang Y and Leng D 2024 *Chem. Eng. J.* **489** 151402
[18] Zhang C 2025 *Chin. Phys. B* **34** 048702